51st AIAA Aerospace Sciences Meeting including the New Horizons Forum and Aerospace Exposition
07 - 10 January 2013, Grapevine (Dallas/Ft. Worth Region), Texas

AIAA 2013-1162

Visualization and Analysis of Vortex Features in Helicopter Rotor Wakes

David L. Kao[1], Jasim U. Ahmad[2], and Terry L. Holst[3]
NASA Ames Research Center, Moffett Field, CA

Brian G. Allan[4]
NASA Langley Research Center, Hampton, VA

Vortex interactions in helicopter rotor wakes are visualized using enhanced flow visualization techniques, which in turn play a crucial role in understanding the dynamics of these complex flows. Iso-surfaces are clipped in a 3D volume to reduce visual clutter. Flow textures are improved to highlight vortical flow structure and vortex-wake interactions. These visualization techniques are applied to three Computational Fluid Dynamics (CFD) simulations of helicopter flow fields. The presented techniques provide a good depiction of rotor tip vortices in these flows.

I. Introduction

In rotorcraft flow fields there are many interesting flow phenomena that arise from complex interactional aerodynamics for both hover and forward flight. A few of these include blade-vortex interactions, vortex pairing, vortex breakdown, vortex-wake interactions and the interaction of various flow features with the fuselage. These flows are typically multidiscipline in nature, with unsteady aeroelastic effects often being present. In a rotorcraft wind tunnel experiment there are additional flow interactions caused by the existence of wind tunnel walls and support hardware. In all these rotorcraft scenarios unsteady, viscous flow dominates.

For all rotorcraft flow fields, those generated via flight, wind tunnel test or numerical simulation, it is important to understand the complex nature of these flow interactions. They can adversely affect rotorcraft aeromechanic and/or aero-acoustic performance in a large number of ways.

An engineer can easily tell if one blade geometry is aeromechanically superior to another at a given flight condition by comparing integrated performance information. For example, Figure of Merit (FM) for hover or normal force (Cn) and pitching moment (Cm) coefficients for forward flight. But it is difficult to tell why the better blade is superior unless more detailed information about the unsteady flow field is available. Likewise, for a rotor blade with superior overall performance (at a given flight condition) it is difficult to tell whether or not its performance is uniformly superior at each blade radius and/or azimuthal angle unless detailed information about the entire unsteady flow field is available.

Having accurate and more detailed information about rotorcraft flow field physics is only part of the problem's solution. The resulting information must be in a format that is analyzable with suitable software tools that are reasonably fast, accurate and easy to use. Since a rotorcraft flow field is extremely complex, typically requiring an unsteady, three-dimensional description, the amount of data needed to describe a single forward flight scenario is massive. Therefore, a graphical approach lends itself as the best solution for interrogating/analyzing these complex and massive databases accurately and efficiently. In many senses the post processing and graphical analysis of these flow fields are as difficult as the data's generation. This paper addresses the topic of flow visualization for complex, vortex-dominated flow fields, like those associated with rotorcraft in hover and forward flight.

---

[1] Researcher, NASA Advanced Supercomputing Division, M/S N258-5.
[2] Aerospace Engineer, NASA Advanced Supercomputing Division, M/S N258-2, AIAA Member.
[3] Branch Chief, Fundamental Modeling and Simulation Branch, NASA Advanced Supercomputing Division, M/S N258-2, AIAA Fellow.
[4] Research Scientist, Flow Physics and Controls Branch, NASA Langley Research Center, M/S 170, AIAA Senior Member.

Many flow phenomena from three-dimensional flow-field simulations can be analyzed and understood using the iso-surface visualization technique—the display of contours of a specific scalar quantity (e.g. pressure or vorticity magnitude) on a three-dimensional surface. This process almost always requires iteration on the quantity being displayed, the contour levels and location and orientation of the viewing surface. Additional processing or manipulation of the iso-surface information can be performed to gain a better or more complete understanding of the flow physics and is a major emphasis of the present paper.

Another use of visualization technology is to aid the process of validation, which typically involves the quantitative comparison of computed and experimental results. There has been a considerable amount of work reported within the experimental research community during the past several years that has involved a number of new and innovative ways for measuring the flow-field characteristics of rotorcraft flows.[1-6] A few of these include Particle Image Velocimetry (PIV), Wide-Field Shadowgraphs, and Laser Doppler Velocimetry (LDV). Advanced visualization techniques can be utilized to compare computed with experimental results that utilize various advanced measurement techniques.

This paper describes the numerical approach for several novel flow visualization techniques, then shows a number of examples using three different rotorcraft simulations and ends with concluding remarks.

II. Approach

The present study uses a variety of visualization techniques to improve the understanding of complex three-dimensional flow fields, especially those associated with unsteady rotorcraft applications. A few of the techniques utilized include: iso-surface extraction, scalar function color-mapped cutting planes, and flow texture mapping. Several of these techniques are used in combination to highlight rotorcraft flow-field features. A more in-depth review of certain features from a variety of baseline visualization techniques is now presented.

A. Baseline visualization techniques

One common method, iso-surface visualization, is to compute and display contours of a suitable scalar quantity (e.g. vorticity magnitude) on a cutting plane. Another common method is to compute and display the actual iso-surfaces of a suitable scalar quantity. Either of these approaches can be used to determine the location and structure of specific features within a flow field.

Other popular flow visualization techniques include: color-mapped grid surfaces based on a scalar quantity, particle traces, and simulated surface oil flows via surface restricted particle tracking and texture flow patterns. Each technique has its pros and cons in terms of its effectiveness in revealing flow details.

In many cases, the flow features revealed by a visualization technique will depend on user-specified parameters. For example, the color map associated with a contour display of a suitable scalar quantity along a cutting plane will determine how much (or how little) of the flow-field structure is revealed. A common method is to use a color map with uniform contour levels based on user-specified minimum and maximum values. However, this method may fail to reveal interesting flow features, especially if the minimum and maximum values have been inappropriately selected. Sometimes, a color map with non-uniform contour levels is more useful. Certain flow features can be enhanced with the careful specification of tailored contour levels.

B. Iso-surface clipping

In rotor wake analysis the rotor tip vortices are typically tracked for their position, size and strength. In wind tunnel experiments, PIV measurements allow a vortex core to be captured at an instance in time on a plane. An example of such a measurement can be found in Ref. 6, where rotor wake behavior over the outer 50% of the rotor radius was measured in a plane. For visualization of numerical results, a similar plane can be placed a short distance downstream of the rotor blade to capture a PIV-like rotor wake.

C. Texture mapping

Flow visualization using particle traces is a common approach in the post processing of flow simulations. Streamlines or streak lines, in practice, are quite common and easy to compute. However, the effectiveness of using streamline flow visualization depends highly on the seed locations, i.e., locations where the streamlines originate.

When the flow along a surface needs to be analyzed, the concept of texture mapping can be used to enhance the display of information. In the scientific visualization community, there have been many visualization techniques that create texture patterns to represent the underlying vector field.[7] A classical algorithm is the Line Integral Convolution (LIC) method, which creates flow-like texture patterns.[8] This visualization technique generates synthetic textures with a surface flow like pattern. Additional discussion in this area is presented in Refs. 9-10. The advantage of using flow textures over streamlines (or streak lines) is that seed placement is not required.

Using the LIC-based texture mapping technique, the surface flow is typically visualized using a monochrome color, but this can easily be enhanced. For a monochrome texture map, the color of the texture is simply the gray scale intensity at that texel, a texture element. Sometimes it is more effective to color the flow texture map using a scalar quantity from the flow field, where the final color texture map is a mixture of the texture intensity and the color derived from the scalar quantity. Several coloring schemes have been proposed.[9] This study evaluates the effectiveness of these schemes in depicting vortices. Let I_t be the grey scale intensity at a texel t, where $I_t \in [0, 255]$. Let C_t be the RGB value at the same texel t based on the scalar flow quantity. The RGB-B (RGB to Black) coloring scheme assigns the output color of the texel (O_t) by varying the RGB value from the C_t color to black using the following equation:

$$O_t = C_t * I_t / 255,$$

where $C_t = (r, g, b)$ at texel t and I_t is the gray-scale intensity at t.

This coloring scheme in general works well if the overall image intensity is bright. However, if the image intensity is darker, then it is preferable to try the RGB-W (RGB to White) coloring scheme, which varies the RGB value to white using the following equation:

$$O_t = C_t + (255 - C_t) * I_t / 255,$$

where $C_t = (r, g, b)$ at texel t and I_t is the gray-scale intensity at t.

A second scheme is the W-RGB-B (White to RGB to Black) coloring scheme, which assigns the output texel color by varying the RGB value from white to the C_t color and then to black according to the following equation:

$$\begin{aligned} &\text{if } (I_t < 128) \\ &\quad O_t = C_t * I_t / 127 \\ &\text{else} \\ &\quad O_t = C_t + (255 - C_t) * (I_t - 127) / 128. \end{aligned}$$

A third coloring scheme is to highlight regions where the flow direction varies locally. This can be achieved by assigning color to the texels in these regions and then use a gray-scale intensity for the rest of the image. To determine how the flow direction changes in a local region, the dot product of the velocity vectors from neighboring texels is computed. This technique is useful for the detection of flow separation and reattachment, especially on the wing upper surface.

In this study, we also propose a new approach that allows the user to specify locations with color textures according to the user-specified scalar quantity. The idea is to use color texture in regions where the scalar quantity is high and monochrome texture in regions where the scalar quantity is low. The regions with low scalar quantity may not be as interesting as those regions where the scalar quantity is high.

III. Results

A. Flow solver

The visualization techniques presented herein are demonstrated using three rotorcraft simulation datasets, which have been computed from the OVERFLOW2 (version 2.2) flow solver, which solves the Reynolds-averaged Navier-Stokes equations. The OVERFLOW2 code was created a decade ago by combining the original OVERFLOW code[11-12] and the OVERFLOW-D code, which was capable of solving the flow over moving geometries.[13-15] The resulting OVERFLOW2 code is a structured flow solver that utilizes the well-known chimera or overset zonal grid approach.[16]

For the OVERFLOW2 overset grid implementation there are two types of structured grid zones: Near-body grids and off-body grids. The near-body grids are curvilinear in nature and conform to solid-body surfaces within the flow field to allow for accurate solid-surface boundary condition implementation—typically no-slip conditions for viscous flow computations. The off-body grids are typically isotropic Cartesian grids that cover the flow regions beyond or outside the near-body grids. They are typically stacked together in a layered or "brick" fashion and successfully coarsened to cover the region beyond the near-body grids until a reasonable distance is achieved where "free-stream" boundary conditions can be applied. The finest off-body grid, which overlaps with the near-body grid zones, is typically called the level 1 off-body grid or the L1 grid. The next finest set of Cartesian grid zones with a grid spacing twice that of the level 1 grid are called level 2 grids, and so on.

The OVERFLOW2 code contains many flow solver and the turbulence model options. For all cases presented herein an implicit, second-order-accurate backward-difference scheme with Newton iteration was used to advance the solution in time. An HLLC upwind approximate Riemann flux scheme with 5th order WENO reconstruction for the inviscid fluxes was utilized for the spatial discretization.[17] Two turbulence models were used for the results examined in this study—the standard two-equation $k-\omega$ SST turbulence model[18] for the first case, one-equation Spalart-Allmaras model[19] with the Detached Eddy Simulation (DES)[20] length scale modification for the other cases. These models produce similar results for the flows studied herein.

For flexible rotor blade cases a structural dynamics module must be coupled with OVERFLOW2 for aeroelastic effects. This is accomplished using the CAMRADII comprehensive analysis code[21] and a time-accurate loose coupling approach that includes the ability to enforce trim conditions.

B. Test cases

The first test case involves the simulated flow about a slowed-rotor compound helicopter model that was tested in the NASA Langley 14x22 foot wind tunnel.[22] In order to match the experiment as closely as possible the geometry used in this simulation consisted of the aircraft, the wind tunnel walls, the model support post and the rotor hub mounting mechanism—the Integrated Rotor Test System (IRTS).[22,23] The simulation utilized herein had an advance ratio μ (M_∞/M_{tip}) of 0.55 and a shaft tilt of -5° relative to the body. The grid system consisted of 92 grid zones with 111 million total grid points. The aircraft is embedded in block grids extended to the tunnel walls with an isotropic spacing of 10% of the rotor blade tip chord. These block grids are extended upstream to the inflow and downstream in the wake with uniform stretching. Flow fields surrounding a compound helicopter—an aircraft with a wing/empennage lifting system and a spinning rotor—are quite complex and, thus, particularly suitable for graphical visualization. The interaction of various flow features on the vertical tail and their contribution to tail buffeting was of particular interest in this study.

The second test case involves the simulated flow about an isolated UH-60A rotor system with a simplified hub in forward flight,[24] which was designed to model the NASA/US Army flight test.[25] The particular case utilized within this study is the level flight BVI case (flight counter C8513), which consisted of an advance ratio of 0.15, a hover tip Mach number of 0.64, a freestream Mach number of 0.096 and a shaft tilt angle of 2.538 deg. The grid system consisted of 53 grid zones with 29 million points. The grid for each rotor blade consisted of three separate grid zones: the main rotor-blade body, a cap grid at the outboard tip, and a cap grid at the inboard root. These grids are embedded in an isotropic Cartesian L1 grid that has a spacing equal to 10% of the rotor blade tip.

The third test case also involves the simulated flow about an isolated UH-60A rotor flow,[26] which was designed to model the NASA UH-60A wind tunnel test.[27-28] The grid system topology for this test case was identical to the second test case. However, the L1 grid spacing was twice as fine (5% of the rotor blade tip chord), which resulted in a total grid size of 370 million points. The freestream Mach number was 0.0975, and the hover tip Mach number was 0.65, making the advance ratio 0.15. There was no fuselage included in this simulation. This flow condition corresponded to an experimental test condition for which PIV data were acquired.[6,26]

C. Visualization using iso-surfaces

When the flow field is visualized using iso-surfaces of a scalar quantity, the threshold value determines the "level of detail" that is displayed. A good scalar quantity to depict vortical flow features is the Q-criterion.[24] Figure 1 shows Q-criterion iso-surfaces in the wake surrounding the compound slowed-rotor helicopter from the first test case. The helicopter geometry with support hardware and surface grid system are shown in Fig. 1a. The iso-surfaces shown in Figs. 1b-d were extracted using three threshold values: 1.0E-5 (green), 1.0E-4 (yellow), and 1.0E-3 (red). As can be seen, most of the vortical flow for this case is generated by the support hardware. A small threshold value for the Q-criterion reveals many vortical flow structures (Fig. 1b), and a large value reveals few vortical structures (Fig. 1d). As the threshold value increases, the internal structure of the vortical flow becomes less visible. A natural question is… "What is the appropriate threshold value for this visualization technique?" Another question is… "How accurately does this visualization technique represent pertinent quantities within the vortical flow?" Both questions are important to consider when post processing a simulated flow field.

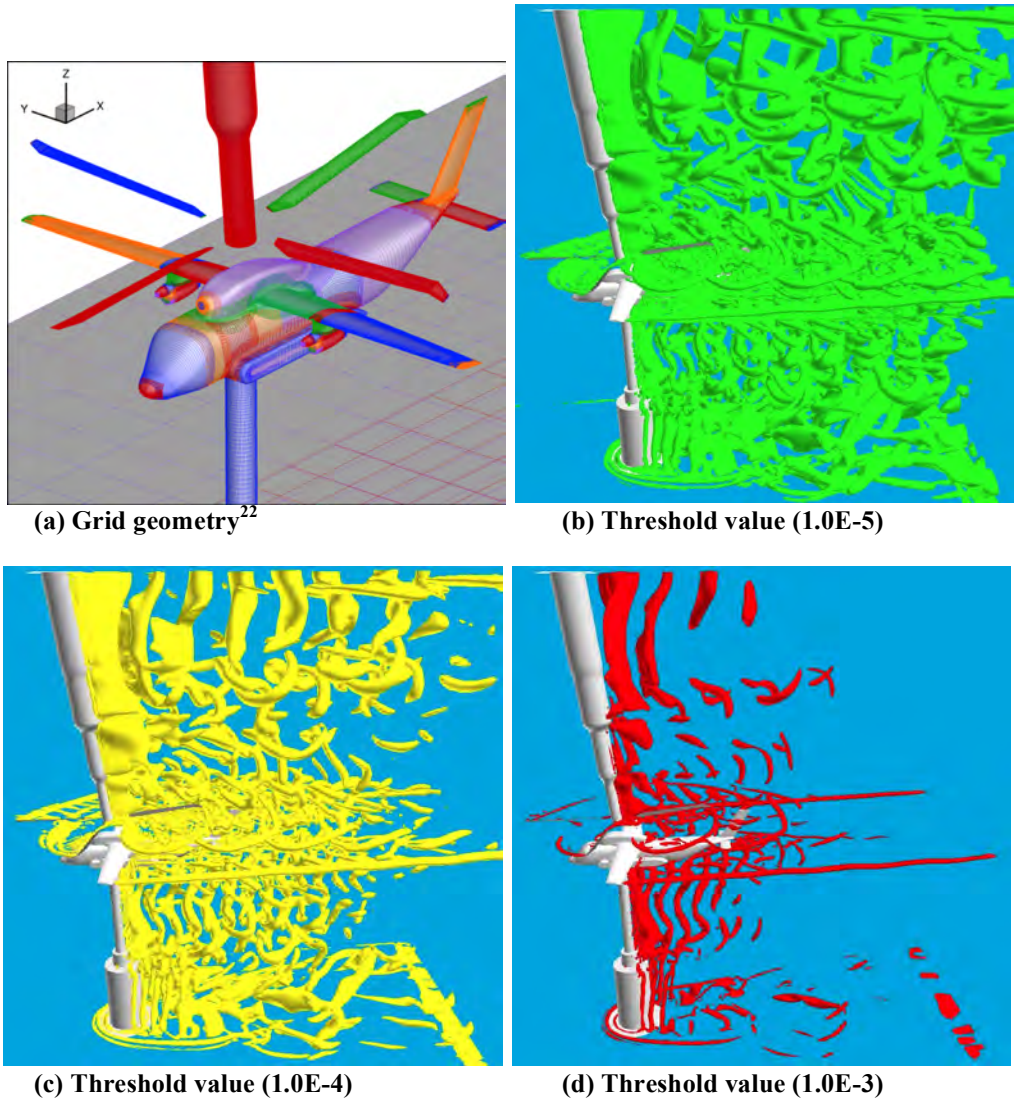

(a) Grid geometry[22] **(b) Threshold value (1.0E-5)**

(c) Threshold value (1.0E-4) **(d) Threshold value (1.0E-3)**

Figure 1. Iso-surfaces of the Q-criterion for a slowed-rotor compound helicopter using three different threshold values, first test case.

A second example of the iso-surface visualization technique, which uses the third test case, is presented in Fig. 2a. Q-criterion iso-surfaces surrounding the UH-60A rotor blades are displayed, only now they are colored by vorticity magnitude. Blade 1 is passing through an azimuth of 90 deg. Using the Fig. 2a viewpoint, Fig. 2b depicts the out-of-plane vertical component in a cutting plane that is parallel to and downstream of rotor blade 1. Contours from this cutting plane are computed from the L1 grid at a distance of 546 mm (0.98 tip chords) downstream of the blade 1 trailing edge. The Fig. 2b image is re-plotted in Fig. 2c using a two-dimensional format. The vertical and horizontal axes are distances in mm measured from the trailing edge point at the blade tip. Using the same scale as Fig. 2c, Fig. 2d shows experimentally measured PIV data.[6] Note the close agreement in vortex position between computation and experiment for the blade 1 vortex (B1), the blade 3 vortex (B3) and the blade 4 vortex (B4). Comparisons between the computed and measured wake positions shed from blade 1 are also in good agreement (B1 Wake). While the position of many features is in good agreement, the computed flow features are more diffused than their experimental counterparts. This is due to numerical diffusion and coarse grid effects, which have already been studied extensively in Holst and Pulliam[29] and Chaderjian.[30]

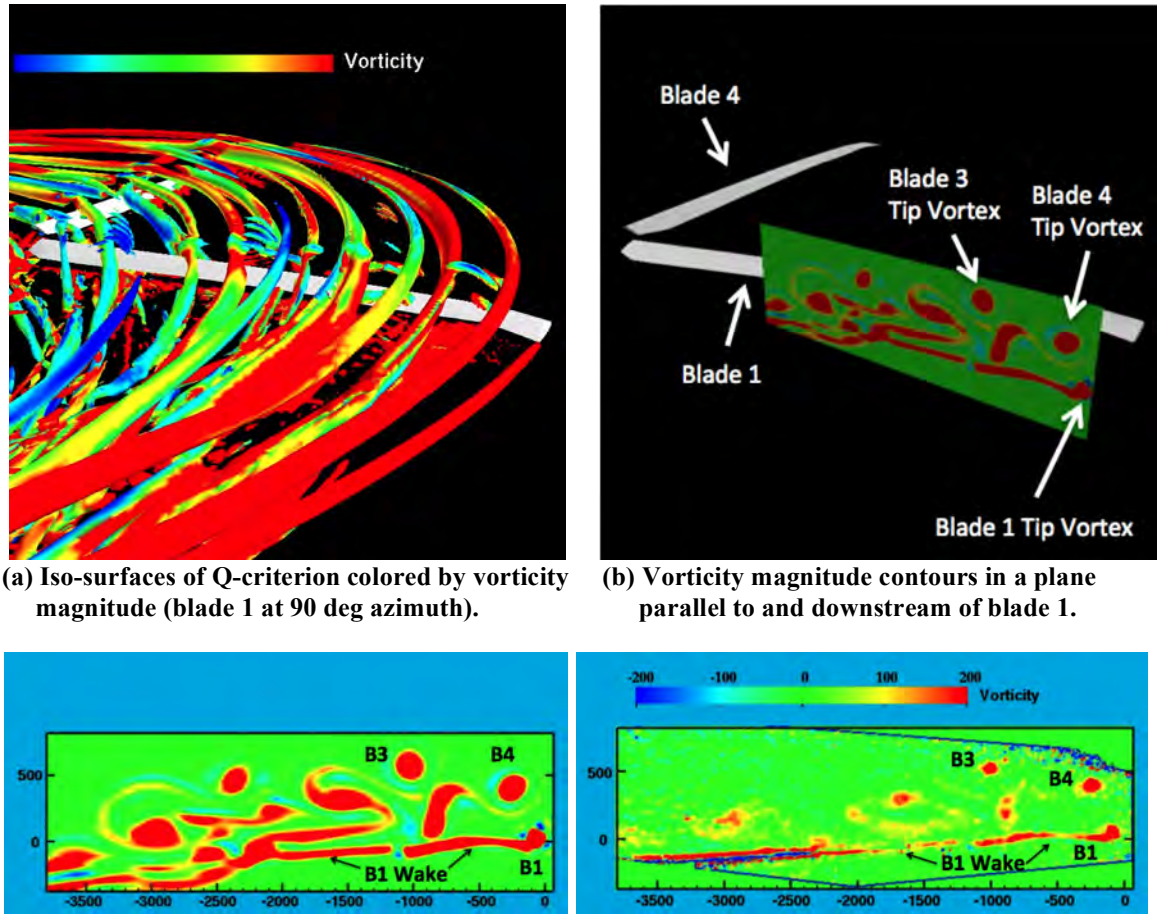

(a) Iso-surfaces of Q-criterion colored by vorticity magnitude (blade 1 at 90 deg azimuth).

(b) Vorticity magnitude contours in a plane parallel to and downstream of blade 1.

(c) Two-dimensional view of Fig. 2(b).

(d) PIV results—same view as in Fig. 2(c).

Figure 2. UH-60A flow visualization using different iso-surface displays with comparison to a PIV experiment, simulation from Ref. 26 (third test case), PIV experimental results from Ref. 6.

The iso-surface technique described above is now demonstrated using a special clipping technique. Figure 3a shows iso-surfaces of the Q-criterion using a threshold value of 0.001 for the first test case. The iso-surfaces are colored by vorticity magnitude. This image shows several flow interactions: vortex shedding along the bottom and upper model supports and the wing tip vortices. There are also flow interactions due to the tip vortices from the rotor blades. Fig. 3b shows a close-up view of Fig. 3a. Due to visual clutter, it is difficult to determine if the rotor tip vortices contribute to tail buffeting.

A method of reducing visual clutter is to associate the iso-surfaces with a scalar quantity. Then, a clipped volume can be used to discard the iso-surfaces that are outside a user-specified range. For the compound aircraft example the iso-surfaces can be colored by their z-coordinate height, which is displayed in Fig. 4a. Using this simple coloring scheme, vortex shedding from four major sources can be seen: upper model support, the rotor blades, the wing tips and the lower model support. Next, a clip volume is chosen so that it encloses the gap between the upper and lower model supports. As a result of applying this clip volume, the iso-surfaces representing the wake structures created by the wing tips and the rotor blades are shown in Fig. 4b. Compared to Figs. 3a-b, Fig. 4b gives a better and less cluttered depiction of the vortices from the rotor blade tips and the wing tips.

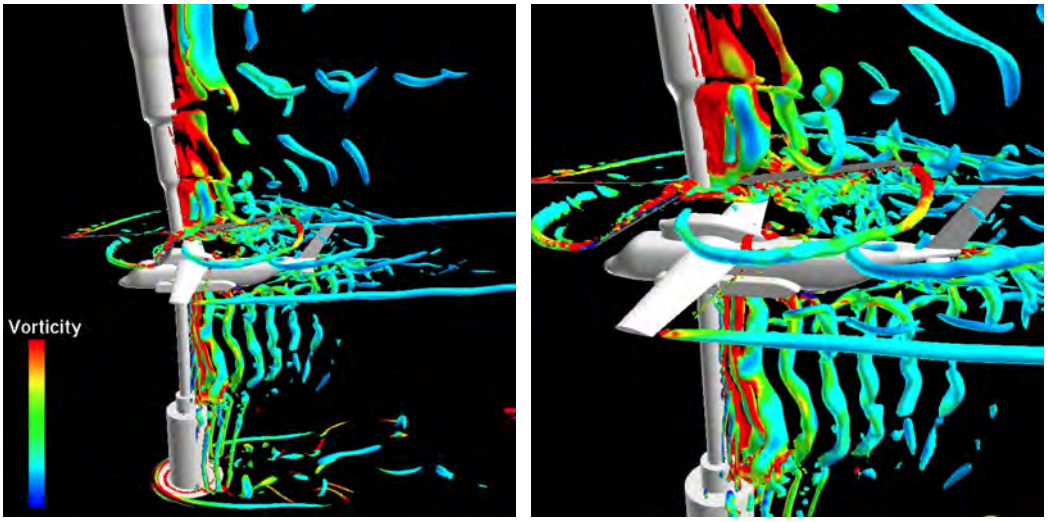

(a) Iso-surfaces of Q-criterion. **(b) Close-up view of Fig. 3(a).**

Figure 3. Iso-surfaces of Q-criterion colored by vorticity magnitude, first test case.

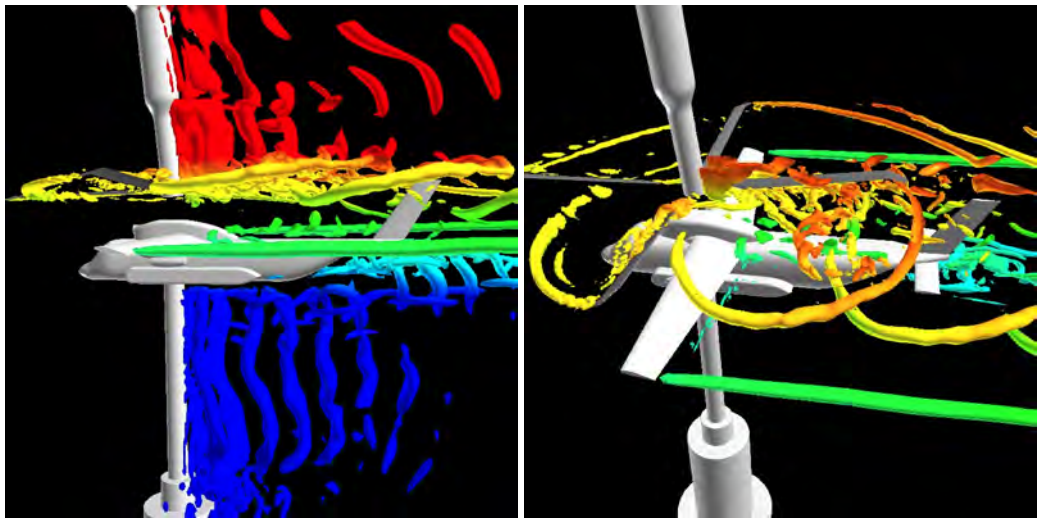

(a) Q-criterion iso-surfaces colored by height. **(b) Clipped iso-surfaces.**

Figure 4. Iso-surfaces of Q-criterion colored to highlight vortices from four geometric components: upper support, rotor blades, wing tips and lower support, first test case.

D. Visualization using texture mapping

Figure 5 compares several coloring schemes using the texture mapping techniques described in Sec. II.C. Each of these views presents flow-field information taken from a cutting plane perpendicular to the freestream, that is downstream of the tail for the compound aircraft test case. Figure 5a depicts the monochrome texture map and Figs. 5b-d depict the texture map with superimposed vorticity magnitude contours using the RGB-B, the RGB-W and the W-RGB-B coloring schemes, respectively. Certain regions of the RGB-B texture map are too dark, while certain regions of the RGB-W texture map are washed out. The W-RGB-B scheme produces the best overall result. Under certain scenarios when the RGB color is not too dark, the RGB-B scheme may be appropriate for depicting various flow features. Figure 6 shows the same flow field as that displayed in Fig. 5, except the texture map is now colored using velocity magnitude. Both coloring schemes, RGB-B and W-RGB-B, give a good depiction of the flow field in this case.

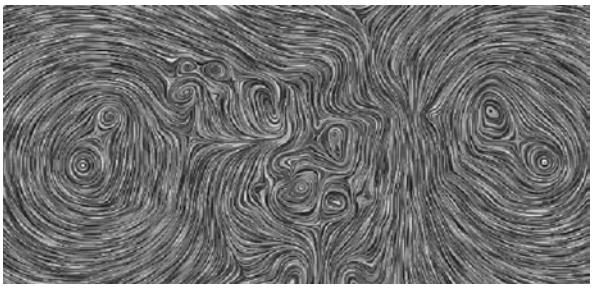

(a) Monochrome flow texture.

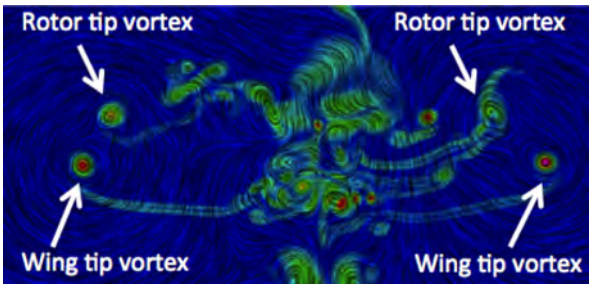

(b) Vorticity magnitude (RGB-B scheme).

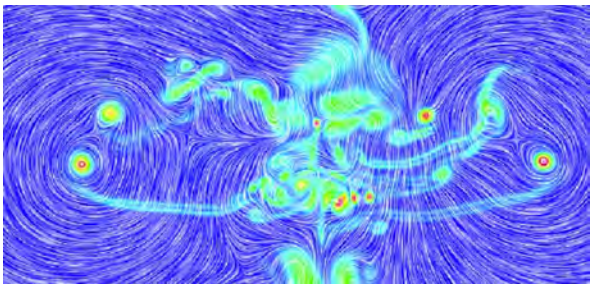

(c) Vorticity magnitude (RGB-W scheme).

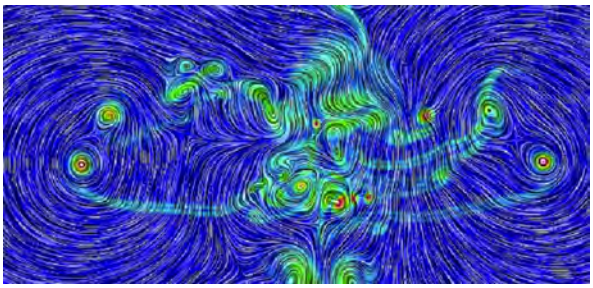

(d) Vorticity magnitude (W-RGB-B scheme).

Figure 5. Comparison of four texture-map coloring schemes based on vorticity magnitude on a cutting plane normal to freestream and downstream of the aircraft tail, first test case.

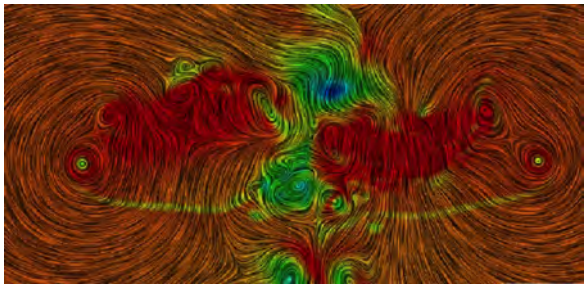

(a) Velocity magnitude (RGB-B scheme).

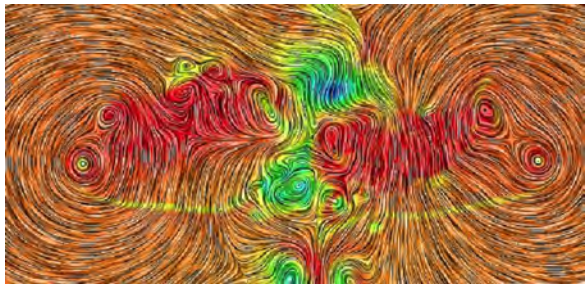

(b) Velocity magnitude (W-RGB-B scheme).

Figure 6. Comparison of two texture-map coloring schemes based on velocity magnitude on a cutting plane normal to freestream and downstream of aircraft tail, first test case.

An additional result showing how a contour plot can be merged with a flow texture map is shown in Fig. 7. In this figure vorticity magnitude contours are merged with a flow texture map for the first test case—the same cross-sectional plane downstream of the aircraft tail that was used in Figs. 5 and 6. The intent in this example is to highlight only those flow regions that contain the highest vorticity. In this regard the texture map is colored using the W-RGB-B coloring scheme, but only when the vorticity magnitude scalar value is above the first contour level, otherwise a monochrome coloring is utilized. The result, comparable with Fig. 5d, shows only that portion of the original flow field with a high vorticity magnitude. In particular, the moderate vorticity magnitude downstream of the wing wake has been eliminated from Fig. 7.

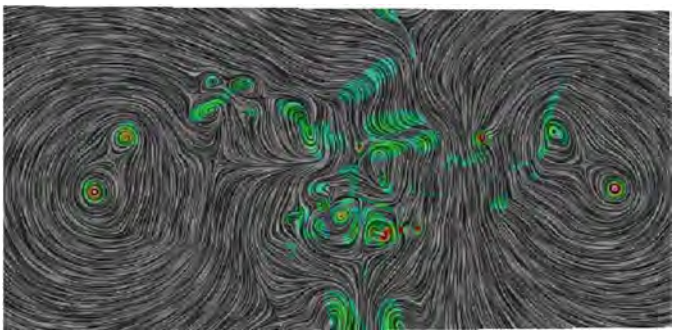

Figure 7. Texture map merged with contours derived from vorticity magnitude using W-RGB-B coloring scheme. Contour levels below first contour level have been omitted. Cutting plane normal to freestream and downstream of the aircraft tail for the first test case.

Another effective visualization technique is to highlight regions with large flow direction variation, which is useful for the detection of flow separation and reattachment. This can be achieved by assigning different colors to each texel in a texture map that is computed from the flow direction variation. Figure 8 shows an example of this using a texture map of the surface flow for the compound helicopter test case. Regions just off the surface with large changes in flow direction are colored red, while the rest of the image is shown in monochrome.

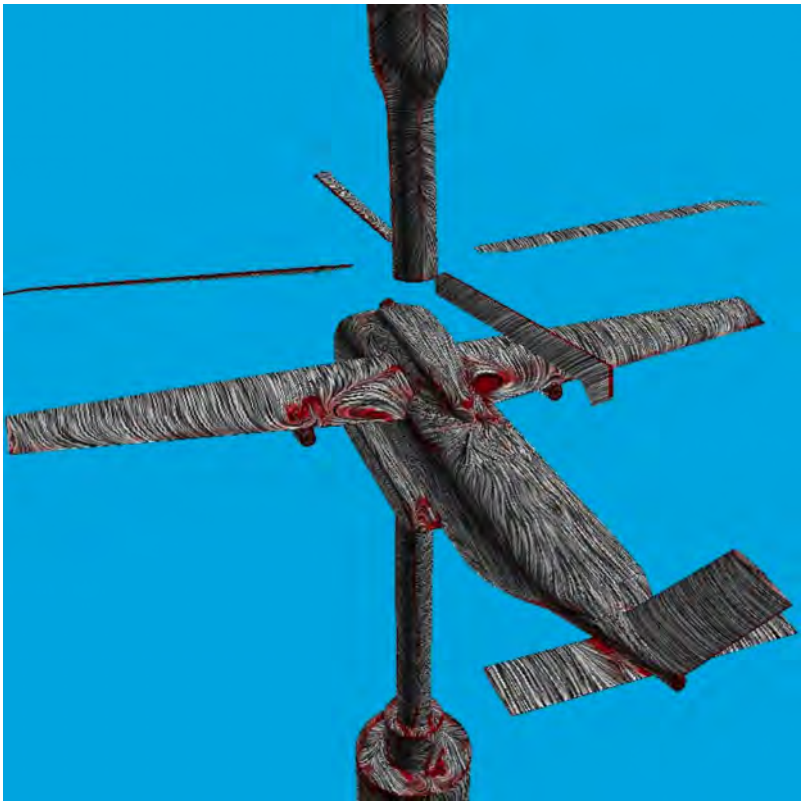

Figure 8. Surface texture map with regions of large velocity direction change highlighted in red, first test case.

Another demonstration of this technique using the second test case (UH-60A, C8513) is shown in Fig. 9. Traditional restricted streamlines are plotted in Fig. 9a for the upper blade surface. A surface texture map with high velocity direction changes highlighted in red (also for the blade upper surface) is plotted in Fig. 9b. The blade in each of these figures is passing through 90 deg azimuth (advancing blade—leading edge is perpendicular to freestream). As can be seen, a separation line near the leading edge extends across most of the length of the blade. This is readily apparent for the texture map (Fig. 9b) but is obvious in the streamline display (Fig. 9a), only near the blade root and tip. The surface streamline depiction of the separation line could be improved, of course, by a more judicious, and typically iterative, selection of streamline release points. This is not required for the texture map when used in conjunction with the velocity direction change sensor. This flow field, as indicated by the blade tip flow separation, has a strong shock near the tip. The reattachment line, which is not apparent in either view, is at the blade trailing edge.

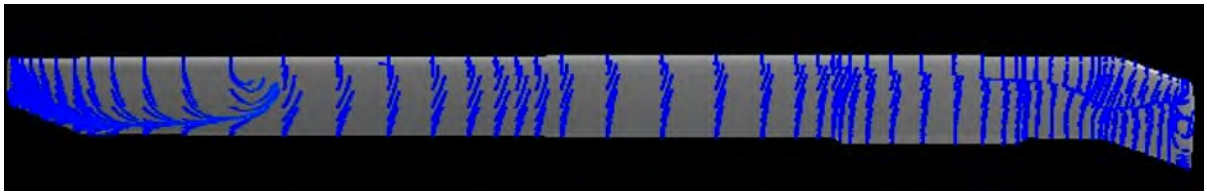

(a) Restricted streamlines.

(b) Texture map. Regions of high velocity direction change highlighted in red.

Figure 9. Comparison of upper surface flow patterns using two different approaches, 90 deg azimuth, second test case.

Next, the flow texture mapping technique is combined with iso-surface clipping to visualize the velocity components on a cross-flow cutting plane for the first test case. Figure 10 shows iso-surfaces clipped in a 3D volume centered at the cutting plane, which is visualized using a cross-flow velocity texture map. The cutting plane is 0.93m downstream from the upper support post. The vortices from the wing and rotor tips—advancing blade on the right, retreating blade on the left—are clearly visible.

Figure 11 shows the cross-flow texture map for the same cutting plane location used in Fig. 10. In this figure dark red textures denote locations where the velocity direction change is maximum, while the monochrome textures indicate regions with little or no change in the flow direction.

Figure 12a shows the vortical flow structure (extracted using Q-criterion iso-surfaces) for the second test case, as the blade is passing through 90 deg azimuth. A cutting plane parallel to and downstream of the rotor blade trailing edge showing a texture mapped cross-flow velocity field is also displayed. Figure 12b shows the same cutting plane view as in Fig. 12a with the iso-surfaces clipped in a 3D volume centered at the cutting plane. With the clipped iso-surfaces the position of the tip vortex is easy to identify. Figure 13a shows the flow texture on the same cutting plane as shown in Fig. 12. Red color textures, for both the cutting plane and the blade surface, denote locations where the flow direction has a high variation. Figure 13b depicts how color textures can be used to highlight locations where the vorticity magnitude is above a user-specified contour level. As shown in Figures 12 and 13, the clipped iso-surface technique and the color flow texture technique are both effective in highlighting vortex features in a given flow field.

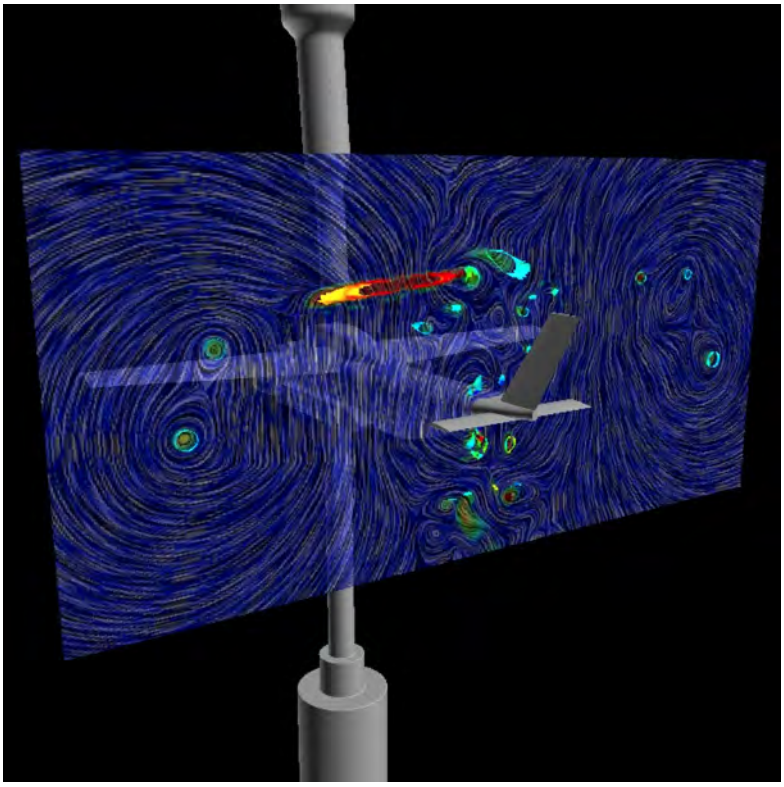

Figure 10. Iso-surfaces clipped in a 3D clip volume centered at the upstream PIV plane, which is textured by the velocity field and colored by vorticity magnitude, first test case.

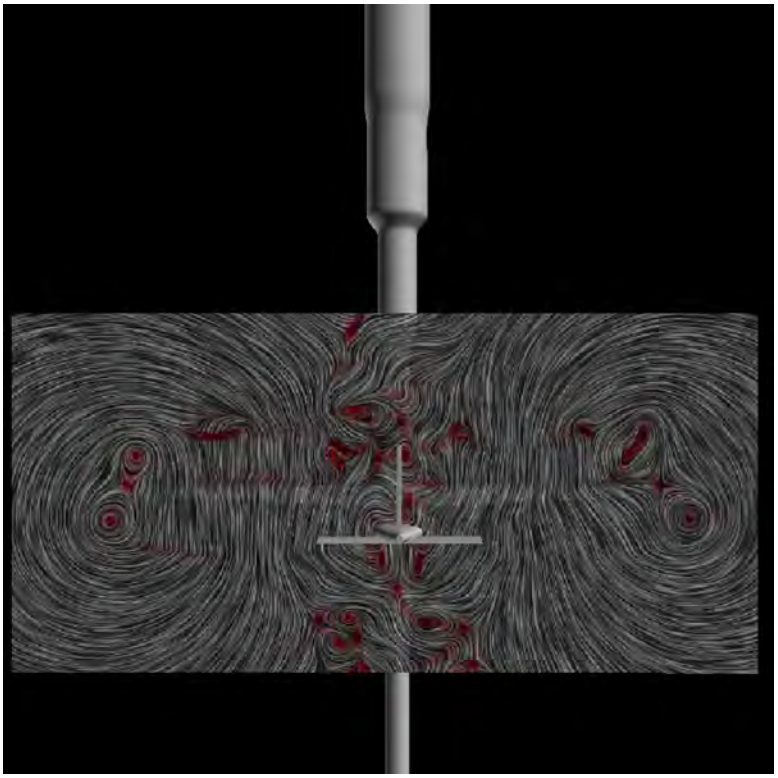

Figure 11. Flow texture depicting cross-flow velocity on the upstream PIV plane, first test case.

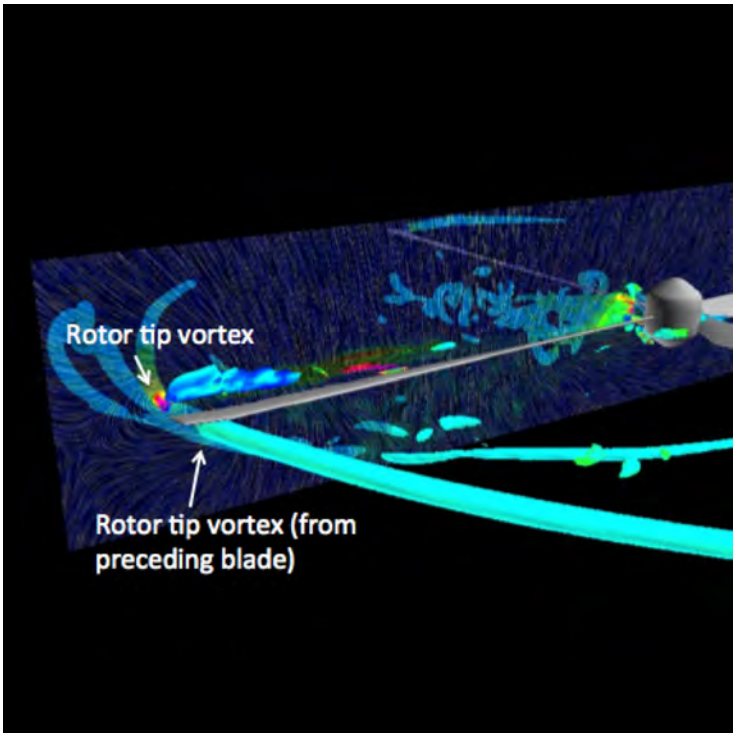

(a) Q-criterion iso-surfaces (threshold value = 0.001) with texture map cutting plane parallel to and downstream of the rotor blade trailing edge.

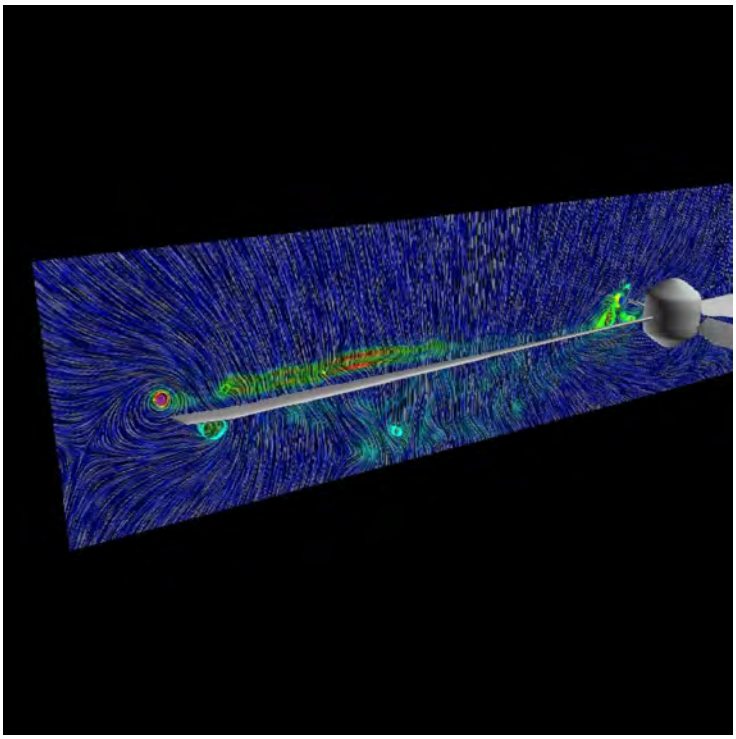

(b) Iso-surfaces clipped in a 3D volume centered at the cutting plane, which is texture mapped and colored by vorticity magnitude.

Figure 12. Comparison of Q-criterion unclipped iso-surfaces and the clipped iso-surfaces downstream of the UH-60 rotor blade system, second test case, blade passing through 90 deg azimuth.

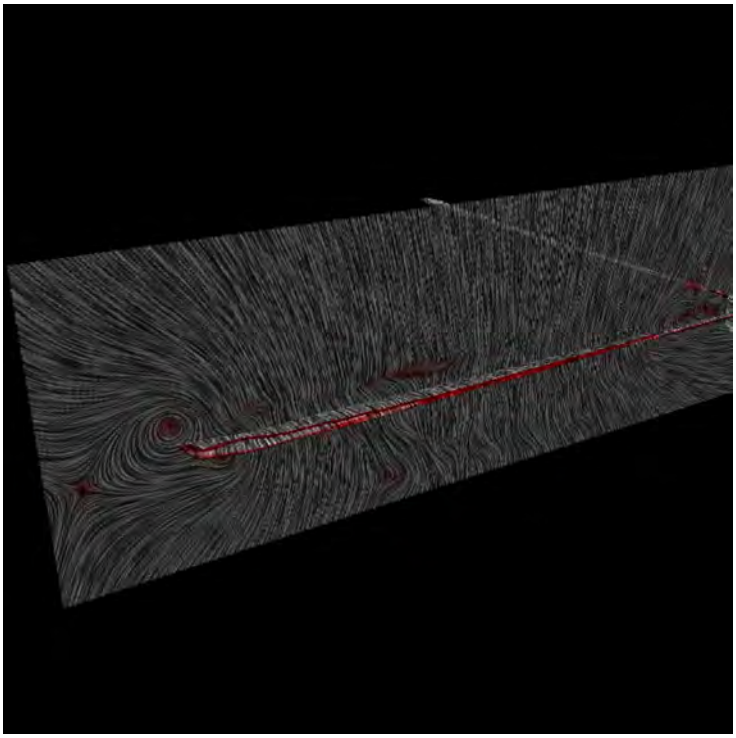

(a) Flow texture—flow direction variation highlighted in red.

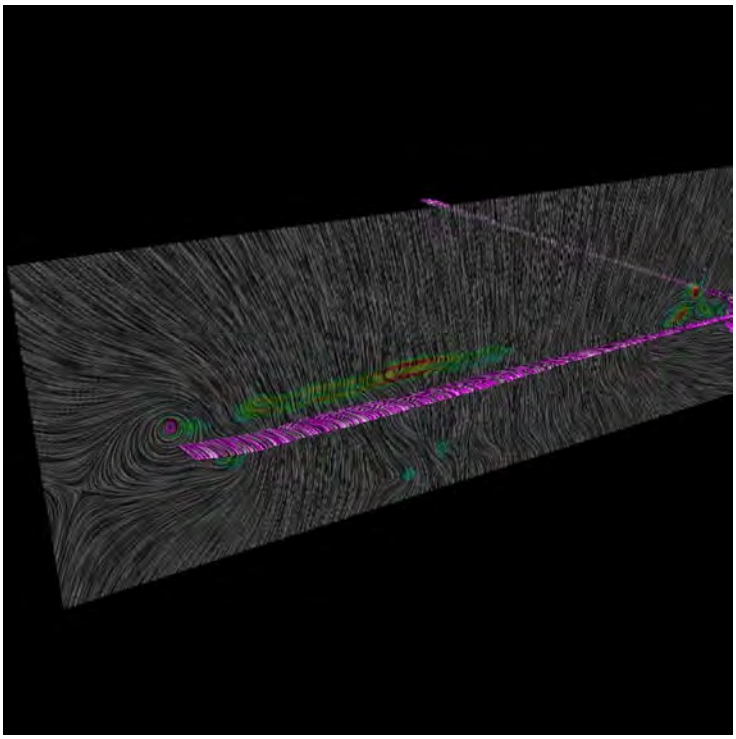

(b) Flow texture colored when vorticity magnitude is above a user-specified level.

Figure 13. Two techniques for highlighting vortex features, second test case.

IV. Concluding Remarks

A number of visualization techniques have been presented to help highlight flow-field features in helicopter rotor wakes. The clipped iso-surface technique was used to reduce visual clutter of traditional iso-surfaces computed from rotorcraft flow fields. The flow texture mapping technique provided an effective way to depict flow patterns on a cutting plane or along aerodynamic surfaces. In one case comparisons with a cutting plane contour map were made with PIV experimental data. Many flow features were easily identifiable with the visualization technique used. Although the numerical features were somewhat diffused relative to the experimental results, the positions of these flow features were in close agreement.

The various visualization techniques have been demonstrated using three rotorcraft CFD simulations: the first for a slowed-rotor compound helicopter, the second for an isolated UH-60A rotor flow designed to mimic a flight test and the third test case for an isolated UH-60A rotor flow designed to mimic a wind-tunnel experiment. All test cases were for forward flight conditions.

A number of visualization techniques combining flow texture mapping with various coloring schemes have also been presented and demonstrated. Flow texture mapping combined with a coloring scheme derived from vorticity was useful for the display of many vortical structures. Flow texture mapping combined with a coloring scheme derived from regions of high velocity direction change proved useful for detecting separation lines.

Acknowledgments

This work was sponsored by the Rotary Wing Project of the NASA Fundamental Aeronautics Program.

References

[1]Leishman, J. and Bagai, A., "Challenges in Understanding the Vortex Dynamics of Helicopter Rotor Wakes," *AIAA J.*, Vol. 36, No. 7, July1998, pp. 1130-1140.

[2]Bhagwat, M. and Leishman, J., "Correlation of Helicopter Rotor Tip Vortex Measurements," *AIAA J.,* Vol. 38, No., 2, Feb. 2000, pp. 301-308.

[3]McAlister, K. and Heineck, J., "Measurements of the Early Development of Trailing Vorticity from a Rotor," NASA/TP-2002-211848, AFDD/TR-02-A001, May 2002.

[4]Mula, S., Stephenson, J., Tinney, C. and Sirohi, J., "Vortex Jitter in Hover," AHS Southwest Region Technical Specialist's Meeting, Feb. 2011.

[5]Ramasamy, M., Paetzel, R. and Bhagwat, M., "Aperiodicity Correlation for Rotor Tip-Vortex Measurements," AHS 67th Annual Forum, May 2011.

[6]Yamauchi, G., Wadcock, A, Johnson, W. and Ramasamy, M., "Wind Tunnel Measurements of Full-Scale UH-60A Rotor Tip Vortices," AHS 68th Annual Forum, May 2012.

[7]Laramee, R., Hauser, H., Doleisch, H., Vrolijk, B., Post, F. and Weiskopf, D., "The State of the Art in Flow Visualization: Dense and Texture-Based Techniques," *Computer Graphics Forum*, Vol. 23, No. 2, 2004, pp. 203-221.

[8]Cabral, B. and Leedom, L.C., "Imaging Vector Fields Using Line Integral Convolution," *Proceedings of ACM SIGGRAPH '93*, 1993, pp. 263-270.

[9]Okada, A. and Kao. D., "Enhanced Line Integral Convolution with Flow Feature Detection," in Visual Data Exploration and Analysis IV, *Proceedings of SPIE 3017,* Feb. 1997, pp. 206-217.

[10]Kao, D. and Shen, H.-W., "Numerical Surface Flow Visualization," AIAA 1988-76, Jan. 1998.

[11]Buning, P., Chiu, I., Obayashi, S., Rizk, Y. and Steger, J., "Numerical Simulation of the Integrated Space Shuttle Vehicle in Ascent," AIAA 88-4359, Aug. 1988.

[12]Renze, K. Buning, P. and Rajagopalan, "A Comparative Study of Turbulence Models for Overset Grids," AIAA 92-0437, Jan. 1992.

[13]Meakin, R., "Object X-Rays for Cutting Holes in Composite Overset Structured Grids," AIAA 2001-2537, June 2001.

[14]Meakin, R., "Automatic Off-Body Grid Generation for Domains of Arbitrary Size," AIAA 2001-2536, June 2001.

[15]Chan, W., Meakin, R. and Potsdam, M., "CHSSI Software for Geometrically Complex Unsteady Aerodynamic Applications," AIAA 2001-0539, Jan. 2001.

[16]Benek, J., Buning, P. and Steger, J., "A 3-D Chimera Grid Embedding Technique," AIAA 85-1523-CP, July 1985.

[17]Toro, E., Spruce, M. and Spears, W., "Restoration of the Contact Surface in the HLL Riemann Solver," *Shock Waves,* Vol. 4, 1994, pp. 25-34.

[18]Menter, F., "Zonal Two-Equation k-w Turbulence Model for Aerodynamic Flows," AIAA 1993-2906, 1993.

[19]Spalart, P. and Allmaras, S., "A One-Equation Turbulence Model for Aerodynamic Flows," AIAA 92-0439, Jan. 1992.

[20]Spalart, P., Jou, W., Strelets, M. and Allmaras, S., "Comments on the Feasibility of LES for Wings and on a Hybrid RANS/LES Approach," First AFOSR Conference on DNS/LES, August 1997, Greyden Press, Columbus, OH.

[21]Johnson, W., "Rotorcraft Aerodynamic Models for a Comprehensive Analysis," 54th AHS Annual Forum, Washington, D.C., May 1998.

[22]Allan, B., Jenkins, L., Yao, C., Bartram, S., Hallissy, J., Harris, J., Noonan, K., Wong, O., Jones, H., Malovrh, B., Reis, D. and Mace, W., "Navier-Stokes Simulation of a Heavy Lift Slowed-Rotor Compound Helicopter Configuration," AHS 65th Annual Forum, May 2009.

[23]Ahmad, J., "Simulation of a Heavy-Lift Slowed-Rotor Compound Helicopter," to be published.

[24]Ahmad, J. and Chaderjian, N., "High-Order Accurate CFD/CSD Simulation of the UH-60 Rotor in Forward Flight," AIAA 2011-3185, June 2011.

[25]Bousman, W. and Kufeld, R., "UH-60A Airloads Catalog," NASA TM 2005-212827, Aug. 2005.

[26]Ahmad, J., Kao, D., Yamauchi, G. and Wadcock, A., "Comparison of Computed and Measured Vortex Evolution for a UH-60A Rotor in Forward Flight," submitted to 31st AIAA Applied Aerodynamics Conference, San Diego, CA, June 24-27, 2013.

[27]Norman, T., Shinoda, P., Peterson, R. and Datta, A., "Full-Scale Wind Tunnel Test of the UH-60A Airloads Rotor," 67th AHS Annual Forum, Virginia Beach, VA, May 2011.

[28]Norman, T., Peterson, R., Maier, T. and Yeo, H., "Evaluation of Wind Tunnel and Scaling Effects with the UH-60A Airloads Rotor," 68th AHS Annual Forum, Fort Worth, TX, May 2012.

[29]Holst, T. and Pulliam, T., "Overset Solution Adaptation Grid Approach Applied to Hovering Rotorcraft Flows," AIAA 2009-3519, June 2009.

[30]Chaderjian, N., "Advances in Rotor Performance and Turbulent Wakes Simulation using DES and Adaptive Mesh Refinement," ICCFD7-3506, Big Island, Hawaii, July 2012.